ELSEVIER

Journal of Structural Geology 26 (2004) 1845–1865

JOURNAL OF STRUCTURAL GEOLOGY

www.elsevier.com/locate/jsg

Foliation development and progressive strain-rate partitioning in the crystallizing carapace of a tonalite pluton: microstructural evidence and numerical modeling

Scott E. Johnson[a,*], Ron H. Vernon[b], Phaedra Upton[a]

[a]*Department of Earth Sciences, University of Maine, Orono, ME 04469-5790, USA*
[b]*Department of Earth and Planetary Sciences and GEMOC Key Centre, Macquarie University, Sydney, New South Wales 2109, Australia*

Received 4 March 2003; received in revised form 9 February 2004; accepted 29 February 2004

Available online 11 May 2004

Abstract

The San José pluton in Baja California, México, comprises at least two well-defined, texturally distinct units. The northern unit was intruded by the central unit after the former had extensively crystallized at its margins. During intrusion of the central unit, the margin of the northern unit underwent brittle and crystal–plastic deformation, at least part of which occurred in the presence of residual melt. We infer that biotite grains in this rock readily deformed by slip and frictional sliding along (001) planes, which caused strain-rate and differential-stress gradients across their grain boundaries into the surrounding plagioclase framework causing it to fracture. These microfractures grew and coalesced, and became sites of localized ductile flow. Continued development of these microshear zones led to coalescence of biotite grains, mainly by mechanical entrainment, and ultimately to a pervasive mylonitic foliation. Thus, in a single deformation, these rocks passed through a brittle–ductile transition. The development of an anastomosing network of ductile microshear zones allowed the progressive partitioning of strain rates, probably over several orders of magnitude, between the microshear zones and intervening polymineralic aggregates.

Numerical experiments were conducted to evaluate the process of biotite-assisted fracturing of the stress-supporting framework, and the progressive evolution of differential stress and strain rate. The results are consistent with experimental evidence that biotite is extremely weak in shear, and that phyllosilicate-bearing rocks may accommodate strain rates several orders of magnitude higher than the bulk strain rate. This study also supports previous suggestions that strain rates associated with the growth of crustal magma chambers may be several, to many, orders of magnitude greater than those normally associated with regional tectonic deformation.

Keywords: Brittle–ductile transition; Foliation development; Intrusion-related deformation; Numerical experiment; Recrystallization; Shear initiation; Strain rate

1. Introduction

This paper investigates the initiation and propagation of microshear zones leading to mylonitic foliation in the deforming carapace of the San José tonalite pluton of Baja California, México (Johnson et al., 2003). Our microstructural observations and numerical modeling results: (1) illustrate the critical role of biotite as the weak mineral in these rocks, (2) are consistent with experimental work on analog materials and mica-bearing rocks, and (3) may provide evidence for fast strain rates during pluton emplacement.

Deformation in rocks is commonly localized into zones of relatively high strain with intervening zones of relatively low strain. This localization occurs at all scales, from intracrystalline dislocations, through intermediate-scale structures such as shear zones and crenulation cleavages, to crustal- and lithospheric-scale structures such as major faults and active tectonic plate boundaries (e.g. Ramsay and Graham, 1970; White et al., 1980; Bell, 1981; Kirby, 1985; Sibson, 1986; Gapais et al., 1987; Hobbs et al., 1990; Jiang and White, 1995; Brown and Solar, 1998; Burg, 1999; Rutter, 1999; Vigneresse and Tikoff, 1999; Ellis et al., 2001; Handy et al., 2001; Goodwin and Tikoff, 2002). Initiation of

* Corresponding author. Tel.: +1-207-581-2142; fax: +1-207-581-2202.
E-mail address: johnsons@maine.edu (S.E. Johnson).

0191-8141/$ - see front matter © 2004 Elsevier Ltd. All rights reserved.
doi:10.1016/j.jsg.2004.02.006

these zones begins at the grain to subgrain scale, associated with heterogeneities that affect the strength of rocks. The range of possible heterogeneities is large, including plastic instabilities, crystalline defects and impurities, lattice preferred orientation, shape preferred orientation, mineralogical variation, incipient melt pockets, and deformation structures (e.g. pre-existing microfractures). Numerous studies in naturally and experimentally deformed rocks and analog materials have addressed the initiation and propagation of ductile shear zones (e.g. Tullis and Yund, 1977; Poirier, 1980; Segall and Pollard, 1983; Segall and Simpson, 1986; Jordan, 1987; Ross et al., 1987; Gottschalk et al., 1990; Hacker and Christie, 1990; Goodwin and Wenk, 1995; Christiansen and Pollard, 1997; Bons and Jessell, 1999; Burg, 1999; Bauer et al., 2000; Goodwin and Tikoff, 2002; Streit and Cox, 2002). However, it remains a relatively poorly understood phenomenon in naturally deformed rocks, owing to: (1) the wide variety of rheological responses of different rock types; (2) incomplete exposure of natural shear zones; and (3) destruction of critical microstructural evidence during progressive (or later) deformation, recovery and recrystallization (e.g. Christiansen and Pollard, 1997; Bons and Jessell, 1999; Handy et al., 2001).

To assess the mechanisms by which ductile deformation initiates and propagates in naturally deformed rocks, it is necessary to track the development of the deformation across natural strain gradients (e.g. Coward, 1976; Van Roermund et al., 1979; Ramsay, 1980; Simpson, 1983; Passchier, 1986; Goodwin and Wenk, 1995). Although such studies can potentially be misleading owing to a lack of knowledge about how strain in these zones was partitioned through time (Means, 1985), their utility may be greatly enhanced if the following conditions can be met: (1) relatively homogeneous and undeformed starting material (e.g. granite), thus avoiding the inherent complication of preexisting anisotropies or deformational fabrics; (2) continuous strain gradient from undeformed host to strongly deformed host; (3) no overprinting penetrative deformation events after shear-zone formation; and (4) preservation of microstructural relations in the most weakly deformed rocks, which are required for identification of key processes of initiation.

These four conditions are rarely satisfied in any single shear zone, but all are met in the San José pluton. The pluton contains a brittle/crystal–plastic deformation gradient within ca. 1 km of its outer margin. Primary igneous microstructure within the pluton is progressively deformed to a mylonitic microstructure near the contact with surrounding host rocks. Of interest to this study, the inner edge of the deformation gradient preserves what we interpret to be evidence for the microstructural processes that initiated the deformation and subsequent fabric development. Thus, the San José pluton provides a natural laboratory in which to investigate microstructural evidence for the initiation and localization of ductile deformation. In the following sections we provide a description of the deformation gradient in the northern unit of the pluton, and show evidence from the least deformed rocks for how deformation may have initiated. We also examine microstructural evidence for evolution of the mylonitic fabric, focusing on the role played by biotite. We then present the results of numerical experiments designed to provide a better understanding of the physical basis for initiation and localization of deformation in mica-bearing rocks. Finally, we discuss various implications of our observations and numerical experiments for pluton emplacement rates and for brittle–ductile transitions during progressive deformation.

In a companion paper (Vernon et al., 2004), we present a detailed microstructural analysis of the rocks across the preserved gradient in brittle/crystal–plastic deformation in the pluton's margin. Vernon et al. (2004) explore: (1) evidence of brittle deformation, (2) evidence of melt-present deformation, (3) recrystallization involving modification of fragments produced by brittle deformation, as opposed to recrystallization induced by ductile strain, (4) evidence of contact melting during submagmatic deformation (Park and Means, 1996), and (5) whether the spatial deformation gradient in the pluton margin reflects the deformation history experienced by the most deformed rocks.

2. The San José pluton and its deformed margin

The 108-km^2-San José pluton is located in the Sierra San Pedro Mártir region of the Jurassic to Cretaceous Peninsular Ranges batholith in northern Baja California, México (Fig. 1; e.g. Gastil et al., 1975; Johnson et al., 1999, 2003). The pluton comprises at least two nested intrusive pulses. On the basis of detailed mapping, microstructural analysis and SHRIMP U/Pb zircon ages, Johnson et al. (2003) concluded that the northern unit was the earliest pulse, and that intrusion of the central unit caused a component of outward expansion of the northern unit, stretching its outer margin. This intrusive history is compatible either with nested diapirism or nested dike-fed growth.

A sharp deformation gradient involving both brittle and crystal–plastic processes occurs within the marginal northern unit (Fig. 2). Tonalite at the inner edge of this unit shows an intrusive igneous microstructure (Fig. 3a). In contrast, rocks at the outer edge of the unit show a mylonitic microstructure (Fig. 3b). The average mode of the marginal northern unit ranges from $Pl_{61}Hbe_{13}Bt_6Qtz_{16}Ksp_{0.13}$ at its inner edge to $Pl_{56}Hbe_6Bt_{10}Qtz_{23}Ksp_1$ at the outer contact with wall rocks (Murray, 1978).

On the basis of detailed structural mapping, geochronology and microstructural analysis, Johnson et al. (2003) concluded that emplacement of the pluton postdated most or all of the regional ductile deformation in the surrounding country rocks. The bulk of the San José pluton—excluding the marginal northern unit—shows a typical intrusive

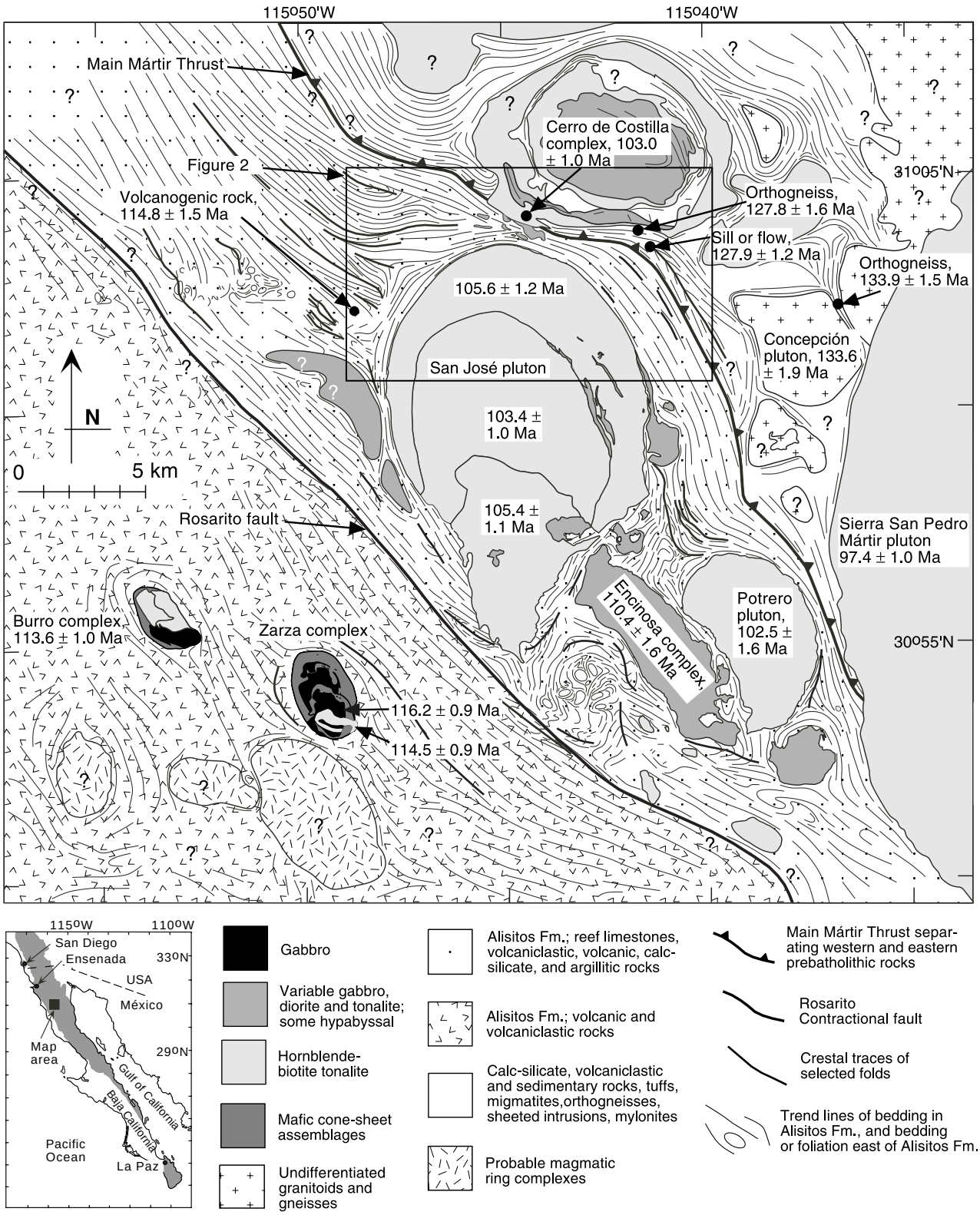

Fig. 1. Geologic map of the San Jose pluton and surrounding region. Map constructed from ground mapping and air photo interpretation. Question marks indicate regions that have not been ground checked. All ages are from SHRIMP U–Pb zircon data reported in Johnson et al. (1999, 2003). See legend for geologic information. Inset map shows the Peninsular Ranges batholith and adjacent prebatholithic country rocks in gray shading.

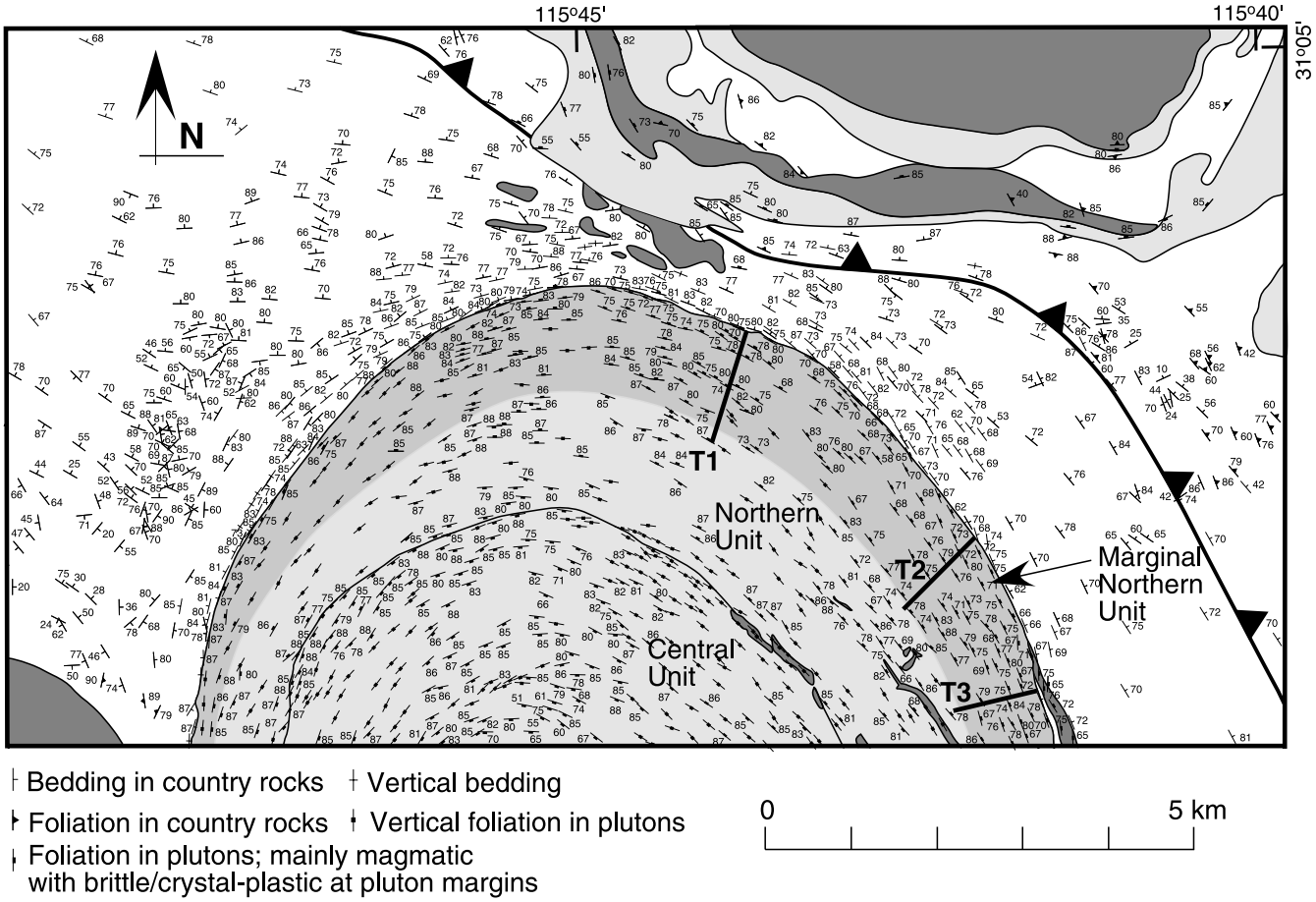

Fig. 2. Map of bedding and foliation data within and surrounding the northern third of the San José pluton. See Fig. 1 for geology legend. Data from principle author and Murray (1978). Marginal northern unit shown in darker shading within the northern unit. T1–T3 are transect lines along which microstructures of the northern marginal unit were investigated.

igneous microstructure (Fig. 3a). Evidence for weak ductile deformation can be found locally throughout the pluton, including undulatory extinction in quartz, mechanical twins in plagioclase, myrmekite in rare K-feldspar, local but minor quartz–quartz grain boundary migration, and variable but minor deformation of biotite (e.g. rare isolated kinks). Evidence for minor fracturing and alteration is also present locally throughout the pluton. These fractures cut across all igneous minerals, and are locally occupied by white mica, chlorite, and epidote. Although the pluton is interpreted as post-kinematic in the sense described above, several kilometers of oblique, brittle/ductile, contractional displacement apparently occurred on the nearby Rosarito fault (Fig. 1) from ca. 100 to 85 Ma (Schmidt and Paterson, 2002). We suggest that the late fracturing and alteration in the pluton may have been associated with this faulting.

Given that pluton emplacement postdates most or all of the regional ductile deformation in this area, the deformation gradient in the northern marginal unit must have formed during pluton emplacement, rather than during an overprinting ductile deformation. Johnson et al. (2003) concluded that this deformation occurred during intrusion of the central unit of the tonalite into the northern unit (Figs. 1 and 2). Contact relations between these two units indicate that they were both magmas at the time of juxtaposition, but the marginal northern unit was at a more advanced stage of crystallization at the time the central unit was emplaced. Vernon et al. (2004) discuss the evidence of melt-present deformation in the marginal northern unit, and conclude that these rocks were probably deformed in the presence of a small amount of residual melt. The strongest evidence noted by Vernon et al. (2004) is the occurrence of fractured, boudinaged plagioclase grains, the boudin necks filled with quartz, microcline and plagioclase that is more sodic than the primary plagioclase (Fig. 3c and d). Some of the deformation may have occurred in the solid state owing to (a) crystallization as the rocks cooled, and/or (b) expulsion of melt owing to partitioning of deformation, with zones of highly non-coaxial deformation forming linked pathways for melt migration (Vigneresse and Tikoff, 1999; Rosenberg and Handy, 2000; Burg and Vigneresse, 2002). Either way, we attribute the sparse evidence for brittle or crystal–plastic deformation in the remainder of the northern unit (i.e. those parts of the northern unit not included in the marginal northern unit) to the presence of sufficient melt to preclude significant grain–grain interactions.

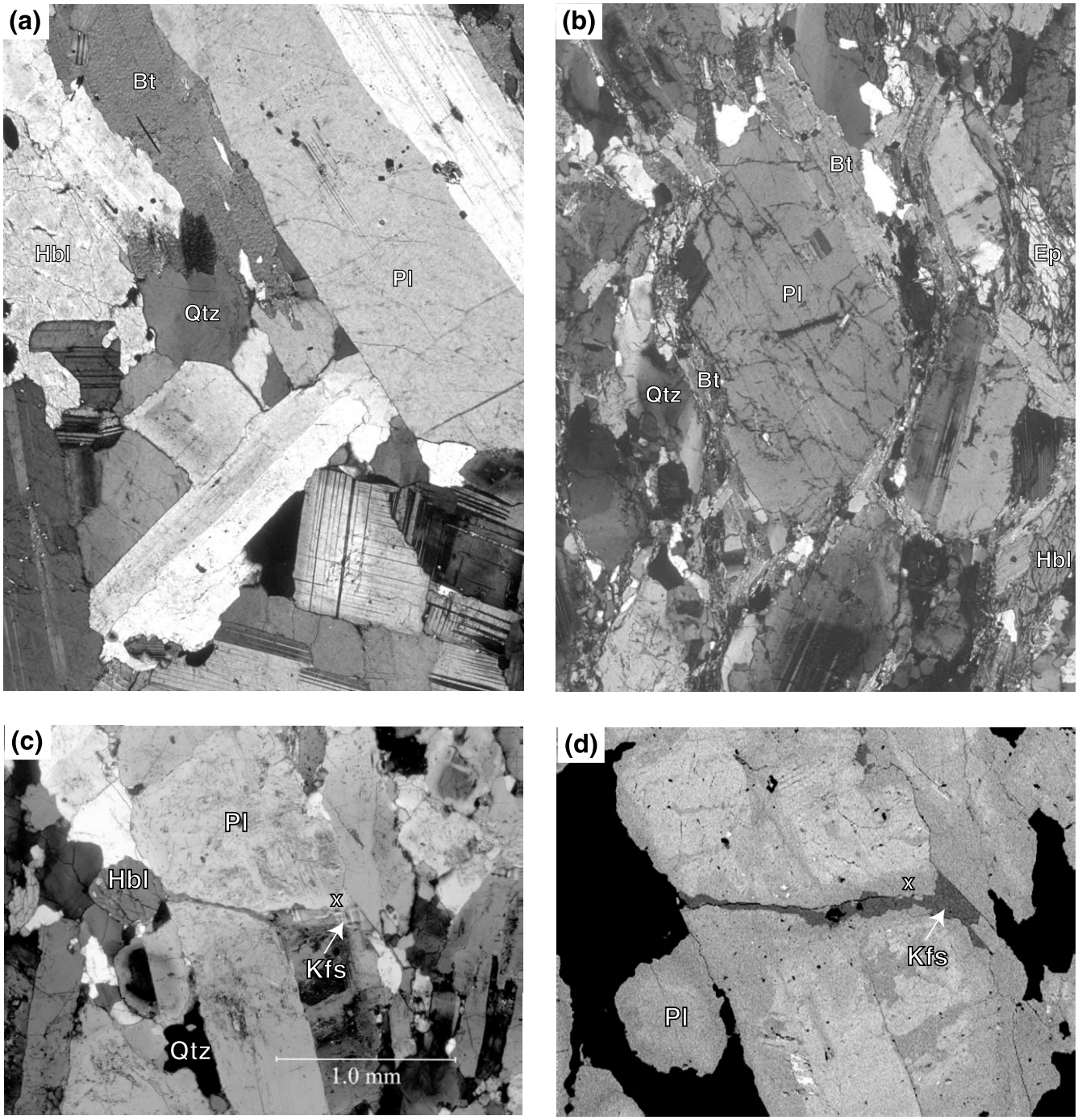

Fig. 3. (a) Largely undeformed tonalite of the northern unit, at the inner edge of the northern marginal unit. The typical intrusive igneous microstructure is only slightly modified. Evidence for possible grain boundary adjustments in quartz and plagioclase, deformation lamellae in plagioclase, and slight bending of biotite all indicate very small strains. Cross polarized light, long dimension of image 1.16 mm. (b) Deformed tonalite at the outer edge of the marginal northern unit, near the contact with the wall rocks. Fractured plagioclase and hornblende, recrystallised quartz, and biotite plus grain-size-reduced feldspar and quartz lining microshear zone are all typical of mylonitic microstructure. Cross polarized light, long dimension of image 2.95 mm. (c) Single-grain of K-feldspar (now microcline) filling a fracture-controlled opening in plagioclase. Clear (inclusion-poor), more sodic plagioclase (x) has crystallized on the walls of the openings, in twin continuity with the primary plagioclase. These areas typically show compositions of An_{23}, whereas adjacent portions of original grain typically show An_{41}. Crossed polars. (d) X-ray aluminum composition map of area shown in (c). Note darker gray color of more sodic plagioclase. See (c) for scale.

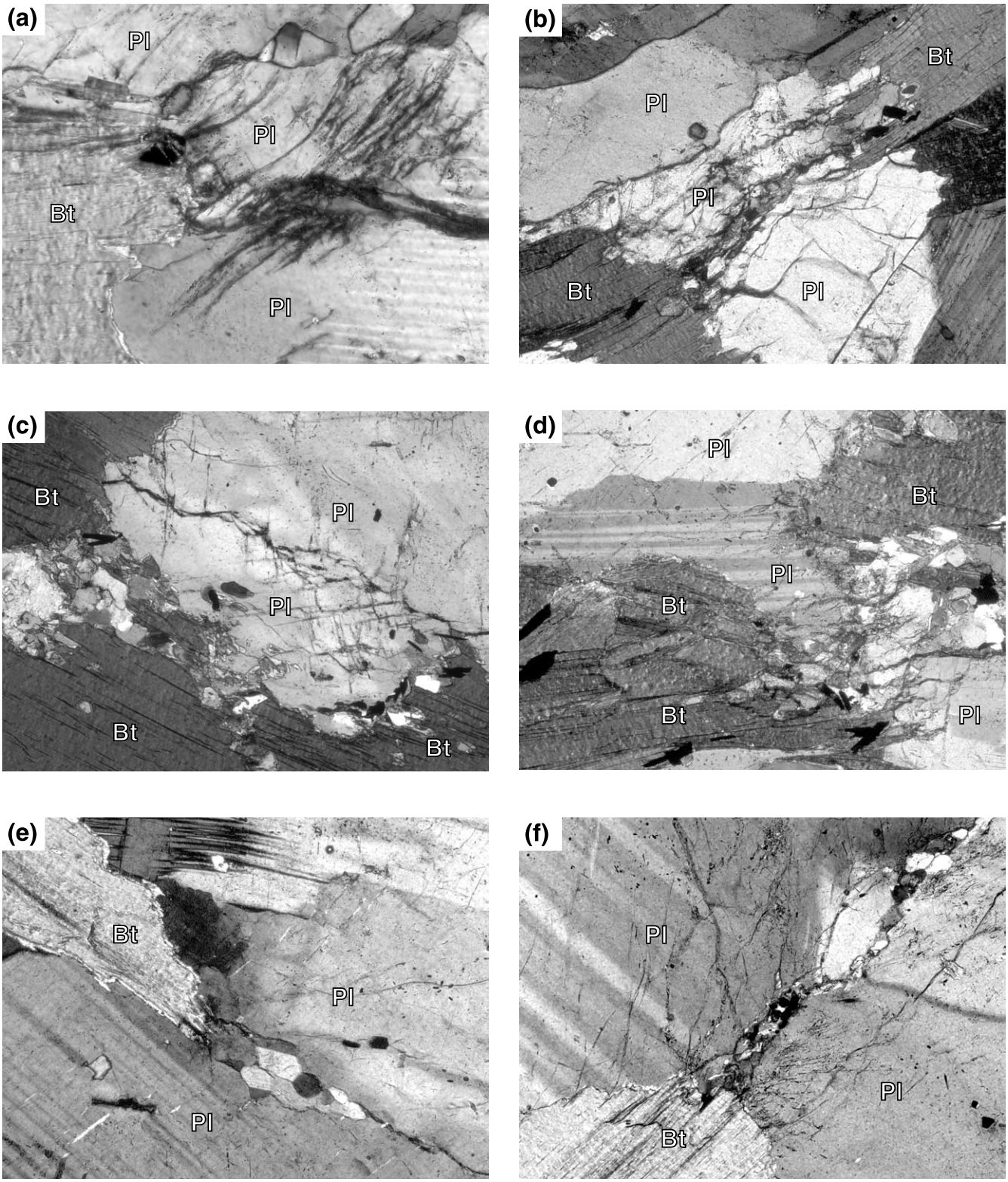

Fig. 4. Photomicrographs from the least deformed portions of the marginal northern unit showing evidence for fracture of plagioclase spatially associated with biotite grains. (a) Curved fractures trending to upper right and lower left, emanating from biotite grain and from east–west-trending shear fracture in plagioclase. (b) Fracturing of plagioclase between two similarly oriented biotite grains. (c) Stepped fracture cutting through the end of a plagioclase grain flanked by biotite grains. Note the parallelogram-shaped segments of plagioclase controlled by the two good cleavage directions, and the patchy misalignment of the plagioclase crystal structure in the fractured area. (d) Fracturing of plagioclase between left-stepping biotite grains. By analogy with experimental results, this would indicate top to the left shear sense. (e) A fracture extending from the tip of a biotite grain. Note the semi-polygonal new grains of plagioclase located in the fracture at the biotite tip, as well as the misorientation in plagioclase crystal structure to the right of the new grains. (f) Fractures in plagioclase extending

In the following two sections we discuss initiation and progressive development of the deformation fabric in the marginal northern unit, focusing on the role played by biotite. A more complete description of the microstructures in these rocks can be found in Vernon et al. (2004).

3. Onset of deformation in the marginal northern unit

Spatially oriented samples were collected at 10–80 m intervals along three transects through the marginal northern unit (Fig. 2): samples were most closely spaced at the outer edge of the unit. Transect lengths vary from 1000 to 1400 m, and were terminated well into the pluton where evidence for brittle or crystal–plastic deformation was no longer observed in outcrop. Two foliation-perpendicular thin sections were prepared from each sample: one parallel to the lineation and one perpendicular. In addition to these transect samples, more than 100 additional samples collected throughout the pluton were examined, which were used by Johnson et al. (2003).

Perhaps the most important observation in the less deformed rocks of the marginal northern unit is that biotite grains are spatially associated with fractures, particularly in plagioclase (Fig. 4). The fractures are both intergranular and intragranular, and in many instances they radiate from the tips of biotite grains much like the splay fractures that form near the tips of small faults. Some of these fractures and their relations to biotite grains resemble shear fractures formed during the experimental deformation of biotite gneiss (Gottschalk et al., 1990; Rawling et al., 2002). For example, Fig. 4a shows a central fracture extending from the tip of a biotite grain, with curved fractures extending both from the biotite grain and the central fracture. These curved fractures resemble 'wing cracks' commonly produced in association with the propagation of mode 2 fractures (e.g. Dey and Wang, 1981; Nemat-Nasser and Horii, 1982; Steif, 1984; Ashby and Hallam, 1986; Horii and Nemat-Nasser, 1986). The fractures are commonly developed where two biotite grains are relatively close to one another, so that the fractures connect the biotite grains (Fig. 4b–d). Some fractures are controlled by the two good cleavages in plagioclase (e.g. Fig. 4c). Others are curved or irregular (e.g. curved fractures in Fig. 4a and d), although these could be cleavage-controlled at a scale too fine to evaluate optically. In some locations, fractured plagioclase at the tips of biotite grains shows evidence for either recrystallization, or sintering of fragments produced during fracturing. These features occur at the tips of single biotite grains (Fig. 4e), and in zones that connect biotite grains (Fig. 4f).

The microstructural evidence suggests that early stages of deformation in the marginal northern unit involved fracture of the framework silicates, particularly plagioclase grains adjacent to biotite grains. Although quartz shows some fracturing, it shows more evidence for dislocation creep. Inelastic strains in biotite were presumably accommodated by slip and frictional sliding along (001) planes (Shea and Kronenberg, 1992). Some fractures also appear to have nucleated on mechanical twins in plagioclase, as investigated in experiments by McLaren and Pryer (2001). The higher occurrence of fracturing in plagioclase as compared to quartz may be explained by the presence of two good cleavages in plagioclase (e.g. Tullis and Yund, 1987). Alternatively, temperature and strain-rate conditions in the marginal northern unit during mylonitic fabric development may have allowed quartz to deform largely by dislocation creep, whereas plagioclase grains were initially required to deform by fracture, followed by recrystallization-accommodated dislocation creep as higher strain rates were localized into microshear zones (discussed later).

4. Coalescence of biotite and development of foliation

After plagioclase fracturing in the marginal northern unit, crystal–plastic deformation localized in the microfractures discussed above to form microshear zones, which coalesced to form a foliation (Figs. 5e and f and 6). Small biotite grains became entrained in the zones of fracturing and grain-size reduced feldspar and quartz, and we suggest that this occurred largely by mechanical 'smearing' of biotite along the microshear zones (Fig. 5a–c), and possibly by crystallization of new biotite grains, although we have no clear evidence for this.

Further deformation led to increased entrainment of biotite into microshear zones, and an increased percentage of grain-size reduced feldspar and quartz (Fig. 5). Although some of the small feldspar and quartz grains may have formed by dynamic recrystallization, feldspar grains commonly show large size variations, and many have sharp corners, straight sides or irregular shapes (Fig. 5d). These features suggest that some/many grains may have originated as fragments that were sintered to resemble new-grain products of recrystallization (e.g. Vernon, 1975; Tullis and Yund, 1987; Stünitz, 1998; Bons and Jessell, 1999; Vernon et al., 2004). Entrainment of plagioclase fragments into microshear zones may have been accompanied by progressive removal of grain corners and asperities (e.g. Figs. 4c and 5d) in a manner similar to that described by Hacker and Christie (1990) in experimentally deformed amphibolite, and by Bons and Jessell (1999) in experimentally

from a biotite grain. The central fracture contains small, new plagioclase grains. Some of these are semi-polygonal in shape. Note large zone of plagioclase lattice misorientation surrounded by fractures in the upper right quadrant. All photomicrographs taken under partially crossed polarizers. Width of (a) is 0.58 mm. Width of (b)–(f) is 1.16 mm.

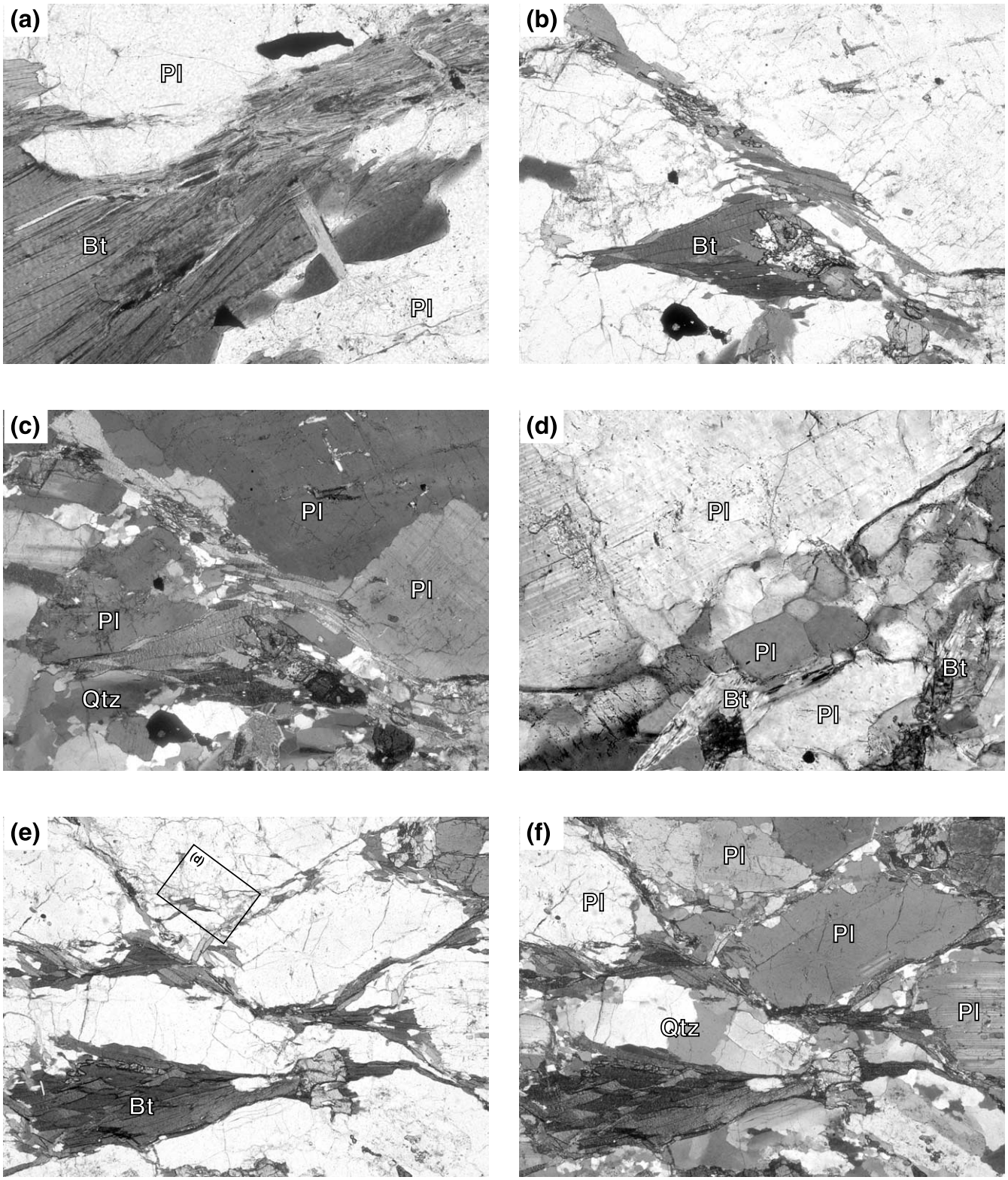

Fig. 5. Photomicrographs illustrating more advanced development of microshear zones. (a) A large, primary igneous biotite grain (lower left) is mechanically shredded and reduced to small, aligned grains leading into a microshear zone. (b) Biotite grains mechanically incorporated into a microshear zone. (c) Same image as (b) under partially crossed polarizers. Note undulatory extinction and new-grain formation in quartz. (d) Magnification of area shown in (e). The corner of this plagioclase grain has been reduced to new grains that appear to have formed as fracture-generated fragments. All grains are lined by fractures, grain-size variation is large, and many grains have straight sides and sharp corners. Grain at lower center has parallelogram shape, much like fracture segments in Fig. 4c. (e) Anastomosing biotite-rich microshear zones defining foliation. The corners of original plagioclase grains have been rounded, and quartz grains have been flattened. (f) Same image as (e) under partially crossed polarizers, showing that biotite is accompanied by grain-size-reduced plagioclase and quartz in the microshear zones that define the anastomosing foliation. Photomicrographs (a), (b) and (e) taken under plane polarized light, (c), (d) and (f) taken under partially crossed polarizers. Width of (a) is 1.16 mm. Width of (d) is 0.58 mm. Width of (b), (c), (e) and (f) is 2.95 mm.

deformed octachloropropane. This is one possible explanation for the rounding of grain edges (Figs. 3b and 5f) and truncation of plagioclase zoning by biotite-rich folia. Most of the boundaries between plagioclase grains in Fig. 5d are microfractures, and one of the central grains (marked 'Pl') has a rectangular shape similar to the fracture-controlled shapes of plagioclase segments in Fig. 4c. Although many of these small grains probably originated by fracturing, the polygonal shapes of some indicate subsequent grain-boundary mobility (Tullis et al., 1990). Thus, the observations suggest a plagioclase microstructure transitional between cataclastic flow and recrystallization-accommodated dislocation creep (Tullis and Yund, 1987). Small new grains are rarely cut by fractures, which suggests that fracturing occurred primarily in the earlier stages of deformation, followed by grain sintering or recrystallization in these narrow zones (Tullis and Yund, 1980; Simpson, 1985; Tullis, 1990).

With increasing strain, biotite continued to act as a weak mineral in the rock, and large igneous biotite grains were destroyed and smeared along developing folia (Fig. 5e and f). This process continued until all the biotite was converted to small, elongate grains defining foliation surfaces (e.g. Mancktelow, 1985). As the fabric developed, quartz continued to deform plastically and eventually formed elongate patches and ribbons. Plagioclase grains also underwent some shape adjustments, presumably through recrystallization-accommodated dislocation creep (Tullis and Yund, 1985). The final product is a continuous, pervasive foliation defined largely by biotite, along with small grains of quartz, feldspar, hornblende, epidote and titanite (Vernon et al., 2004). This foliation wraps larger, less deformed grains of plagioclase and hornblende, and resembles a relatively low-strain mylonitic fabric (Fig. 5e and f).

Fig. 6 shows the fabric evolution from least deformed to most deformed rocks, and illustrates the progressive smearing and coalescence of biotite to define a foliation. Although this is a polymineralic rock, the progressive evolution is markedly similar to processes documented in two-phase solid aggregates incorporating one weak and one strong phase (e.g. Jordan, 1987; Ross et al., 1987; Bons and Cox, 1994; Bons and Urai, 1994). The progressive coalescence of biotite, and the occurrence of biotite as the only mineral in many microshear zone segments, suggests that biotite was the weakest mineral and played a leading role in localization of shear and subsequent foliation development.

5. Numerical experiments

5.1. Description of model

To investigate the initiation of brittle/crystal–plastic deformation in these rocks and the role of biotite in this process, we conducted a series of numerical experiments to simulate the non-coaxial deformation of mica grains within a homogeneous matrix. The physical model is a box with dimensions $x = 5y = 5z$ (Fig. 7a). The box contains 33,135 gridpoints and 27,968 polyhedral elements. Within this box we defined a volume of tight grid-point spacing with dimensions $x = 8$, $y = 5.7z$. Within this inner volume we distributed eight regions defined as biotite grains. These grains have dimensions $x = 2.2y = 5.5z$. The choice of biotite positions was governed by our interest in evaluating the interaction of biotite grains in right-step, left-step and end-on geometries (Fig. 7a). Segall and Pollard (1980) and Dey and Wang (1981) examined the interaction of stress perturbations around variably oriented cracks in an elastic continuum subjected to deviatoric stresses. They found that stress concentrations in the regions between cracks were sufficient to cause crack linkage (e.g. Nicholson and Pollard, 1985; Lin and Logan, 1991). We sought to explore analogous failure linkages between biotite grains, as well as stress variation, strain-rate distribution and distribution of failure linkages during progressive deformation.

Velocity boundary conditions are consistent with a general shear box, as shown in Fig. 7b. These velocities lead to a bulk tensor shear strain $e_{13} = e_{31} = 0.0055$ at 1000 steps. After initializing the velocity structure throughout the model, the velocity conditions were fixed only on the model boundaries. Thus, the interior of the model could deform freely, provided the boundary conditions and continuity were satisfied. In order to avoid the boundaries in our analysis, Figs. 8–10 are central XZ sections through the inner volume shown in Fig. 7a and b.

In our model the matrix was defined as a pressure-dependent Mohr–Coulomb material ($\phi = 50°$—typical value for granite; Lama and Vutukuri, 1978, table 5), and the biotite grains were defined as a modified Drucker–Prager material. Post-failure plasticity in these constitutive models is governed by a shear yield function and a non-associated flow rule (Vermeer and deBorst, 1984). We could have constructed a more complex model involving different constitutive relations, but we chose to use a relatively simple model that was easily interpreted. Although this is an unsatisfactory model for evaluating the microstructural evolution of polymineralic rocks, we have found it instructive in our investigation of deformation in the marginal northern unit.

To apply the Drucker–Prager criterion, a shear strength was assigned for a specific temperature and strain rate using the power law constitutive relations determined by Kronenberg et al. (1990a) for single biotite crystals shortened at 45° to (001), parallel to [100] and [110]. To simulate the environment at the margin of the pluton, we ran our experiments at a confining pressure of 270 MPa corresponding to a depth of ca. 10 km (S.E. Johnson, unpublished aluminum-in-hornblende data), and temperature and strain rate of 650 °C and $10^{-10}\,s^{-1}$, respectively. The notable insensitivity of the biotite flow law to temperature and strain

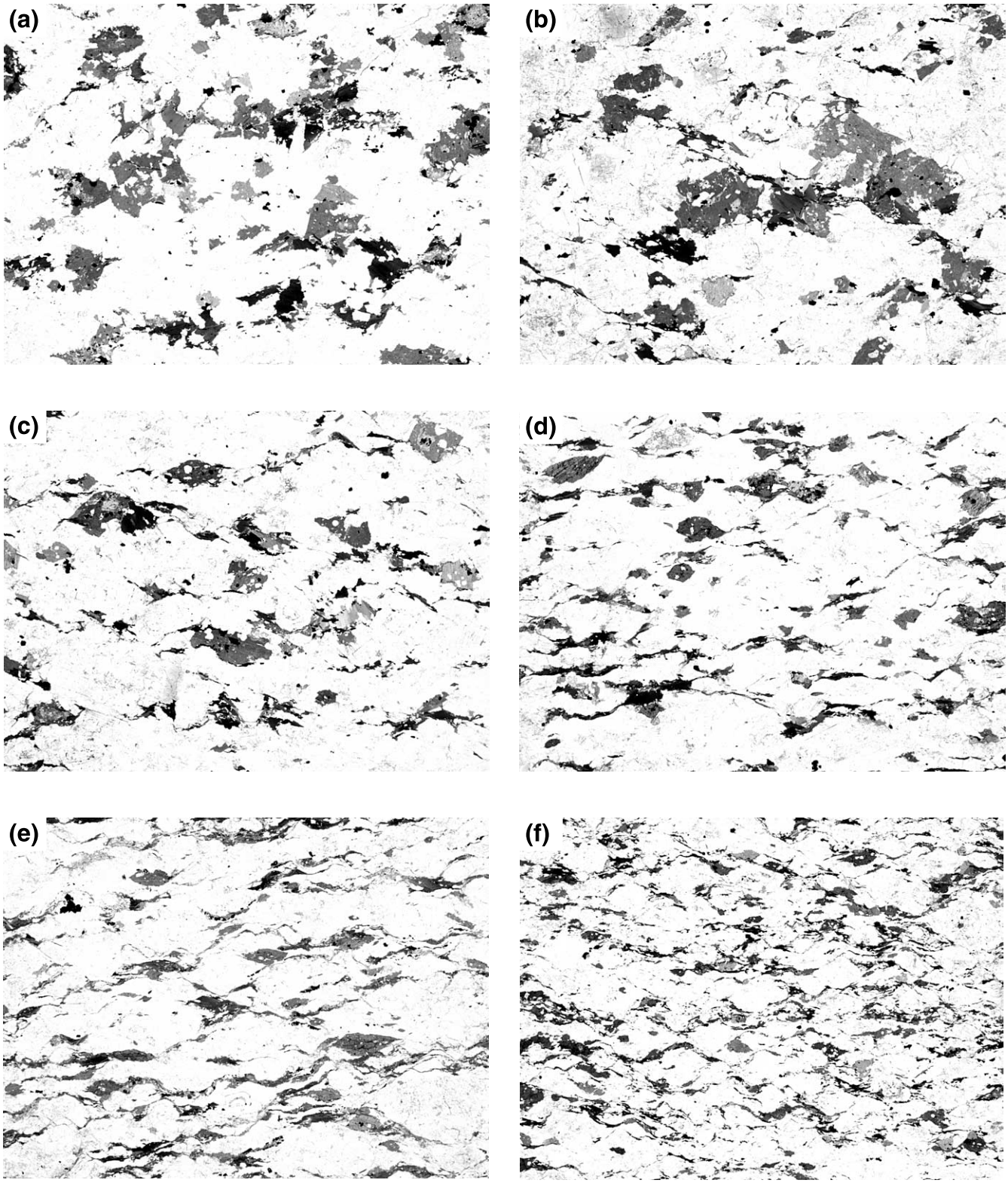

Fig. 6. Sequence of photomicrographs showing progressive fabric development in the marginal northern unit. The igneous microstructure in (a) is only mildly affected by the deformation apparent in (b), where elongate stringers of biotite mark developing microshear zones. The final product in (e) and (f) is a mylonitic foliation. All photomicrographs taken under plane polarized light. Width of all is 26.5 mm.

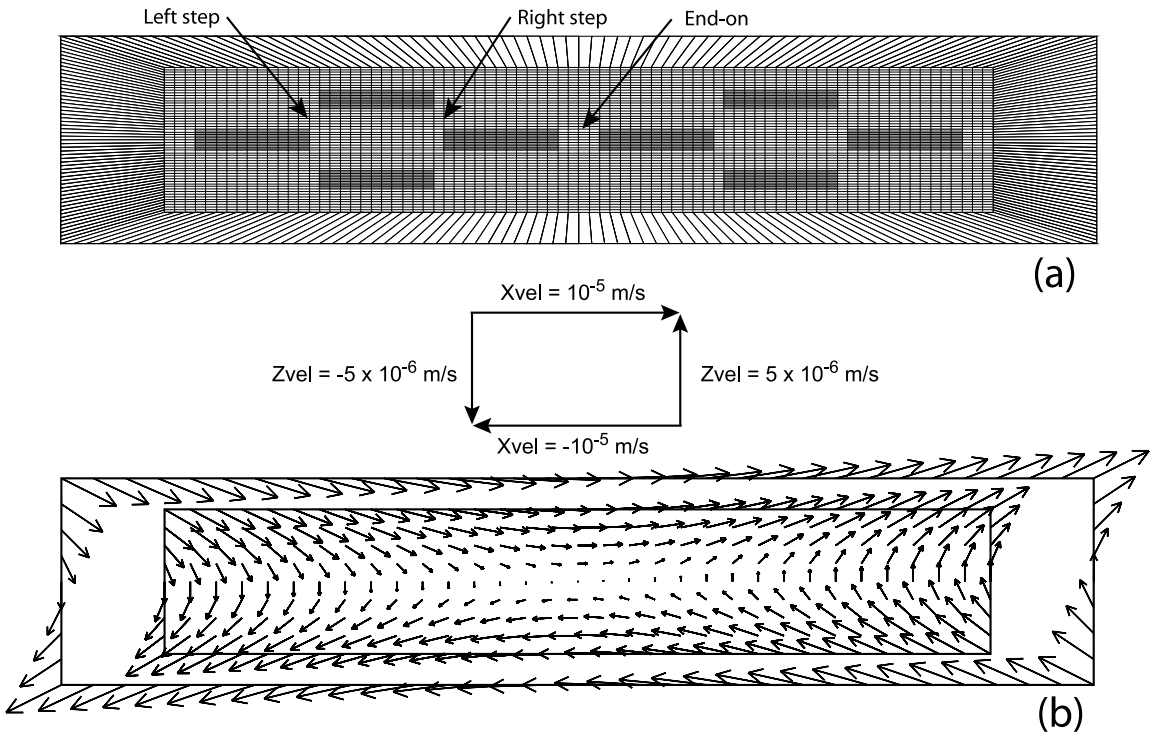

Fig. 7. (a) Central section through the physical model used in the numerical experiments. Eight dark rectangles simulate biotite grains. (b) Same central section through model as in (a), showing the velocity boundary conditions. Arrows are particle velocity vectors for a bulk dextral non-coaxial flow.

rate (Kronenberg et al., 1990a) made precise assignment of these two parameters unnecessary; these values resulted in a shear strength of 9.45 MPa for the Drucker–Prager material.

The mechanical equations were solved in three dimensions using a velocity-based, Lagrangian formulation (FLAC^{3D}; Itasca Consulting Group, Inc., 2002) that uses an explicit finite-difference solution for elastic and plastic behavior. Materials in FLAC^{3D} are represented by polyhedral elements within a three-dimensional grid, each element responding to applied velocity or stress boundary conditions by a prescribed constitutive law. FLAC^{3D} is an extension of the two-dimensional code FLAC, which has been used to evaluate a number of deformation processes relevant to structural geology (e.g. Passchier and Druguet, 2002 and references therein).

5.2. Results of numerical experiments

Figs. 8–10 show failure distribution, differential stress and shear strain rate, respectively, for seven stages between 400 and 1000 steps (the biotite failed almost instantaneously, around step 30). At step 400, the Mohr–Coulomb matrix has failed at the upper-left and lower-right corners of the biotite grains. This result is consistent with theoretical and experimental work on tensile fracture of material around cracks subjected to differential stress (e.g. Segall and Pollard, 1980; Dey and Wang, 1981; Nemat-Nasser and Horii, 1982; Kranz, 1983; Steif, 1984; Ashby and Hallam, 1986; Horii and Nemat-Nasser, 1986). The shear strain rate within individual biotite grains was partitioned during the early stages of deformation, with the highest rates at the grain edges, leading to two zones of high strain rate in each grain.

At step 500, the failure zones between right-stepping biotite grains have linked to form continuous zones of plastic flow (Fig. 8). The strain rate has further partitioned into the biotite grains, and differential stress gradients around the grains have increased. The region between the end-on biotite grains has begun to fail in shear, owing to a rapid increase in the differential stress.

From steps 600 to 650, matrix failure between the end-on biotite grains has linked, completing a long, diagonal region of plastic flow that links four biotite grains across three matrix bridges. Differential stress magnitudes in the matrix away from the zones of localized failure continue to rise concomitantly with increasing strain rates in the linked zones of plastic flow.

At step 700, the failure distribution has rapidly evolved, establishing the essence of a pattern that is maintained with little change for at least 16,000 steps (the experiment was stopped at that point). From steps 850 to 1000, a quasi-steady failure distribution is established; nearly all matrix strain rates outside the linked zones of plastic flow have fallen below $5 \times 10^{-6}\ s^{-1}$, and all right-stepping biotite grains are linked into three zones of high strain rate. At step 1000, shear strain rates reach a maximum value of $1.15 \times 10^{-4}\ s^{-1}$ and a minimum value of ca. $3 \times 10^{-7}\ s^{-1}$. These values are approximately 1.6 orders of magnitude higher, and 1.2 orders of magnitude lower, respectively,

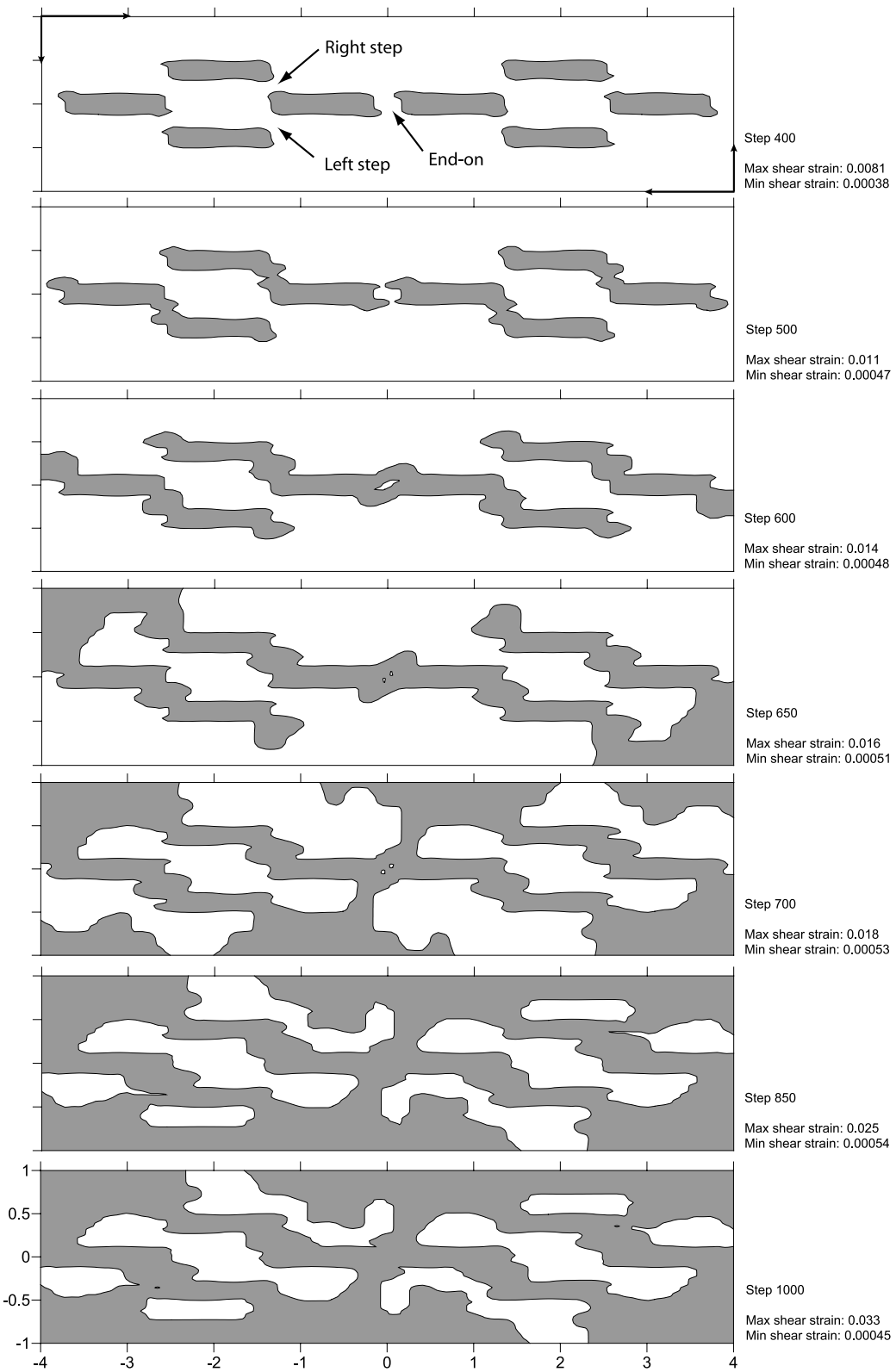

Fig. 8. Failure distribution in central sections through the numerical experiment at seven stages between steps 400 and 1000. Darker shading denotes areas in the model that have failed and are therefore deforming by plastic flow. Biotite fails very early (around step 30), and by step 400 the surrounding matrix begins to fail at the upper left and lower right margins of the biotite. The failure distribution progresses until it reaches a quasi-stable form at step 1000. The white areas at step 1000 have not reached failure, so consequently behave elastically.

than the initial shear strain rate of $5.5 \times 10^{-6}\ s^{-1}$. Because deformation is focused into narrow bands, the average drop in strain rate throughout the matrix is much less than the average increase in the zones of high strain rate.

This history of progressive stress and strain rate partitioning is shown in Fig. 11. The initial distribution of strain rate and stress is nearly uniform and homogeneous. At approximately step 30, the biotite grains begin to fail and flow plastically (point D). This causes a rapid increase in strain rates in the biotite grains, resulting in marked strain-rate and differential-stress gradients across their boundaries with the matrix material. Strain rates increase in matrix zones of linked failure that connect the biotite grains (point C) at approximately step 600, and fall less markedly in other parts of the surrounding matrix (point B). The stress between the two central biotite grains (point A) climbs rapidly. At failure, area A flows plastically at an increasing rate, to approximately step 950. Strain rate differences between the linked failure zones and the surrounding matrix span a maximum of approximately 2.8 orders of magnitude at step 1000, and nearly 2 orders of magnitude at the points shown in Fig. 11.

5.3. Implications of experiments for microstructural interpretations

The model results suggest that instantaneous strain-rate variations between biotite and plagioclase result in high differential stresses in plagioclase grains causing them to fracture. This interpretation is broadly consistent with theoretical (Jordan, 1988; Handy, 1994; Handy et al., 1999) and numerical (Tullis et al., 1991; Bons and Cox, 1994) models of two-phase systems, as well as experimental deformation of polymineralic rocks (Tullis and Yund, 1977; Gottschalk et al., 1990; Holyoke and Rushmer, 2002; Rawling et al., 2002; Tullis, 2002) and two-phase analog materials (Jordan, 1987; Ross et al., 1987; Bons and Cox, 1994; Bons and Urai, 1994). Although we cannot prove that the microfractures in the marginal northern unit of the pluton originated in this way, the lack of these microfractures in the bulk of the pluton, and their progressive evolution into microshear zones and foliation in the more deformed parts of the marginal northern unit, support this interpretation.

Our model geometry incorporated approximately 20% of the weak phase (biotite), and in this instance the strong stress-supporting matrix determined the bulk strength of the experiment in the early stages of deformation (e.g. Tharp, 1983; Jordan, 1988; Handy, 1990, 1994). It is important to note that the maximum tensor shear strain in the zones of linked failure at step 1000 in our numerical experiment is only 0.033 (Fig. 8). Thus, the experiment does not address the issue of coalescence of biotite at higher strains. However, the strain rate partitioning in the experiments is controlled by the weak phase, and we speculate that the linked zones of plastic flow established by step 1000 are ideal candidates for zones of physical and chemical linkage of individual biotite grains and other fine-grained minerals, as observed in the marginal northern unit of the pluton. The smearing and coalescence of weak minerals in the marginal northern unit of the pluton would have caused a marked change in the pattern and magnitude of stress and strain-rate partitioning. Layers composed of weak minerals preferentially strain at lower creep stresses and higher strain rates, leading to weakening of the whole rock (e.g. Price, 1982; Jordan, 1987; Ross et al., 1987; Handy, 1990, 1994; Bons and Cox, 1994).

6. Discussion

6.1. Brittle–ductile transition during progressive deformation

Rocks in the marginal northern unit of the San José pluton appear to record a transition from dominantly brittle failure to dominantly ductile flow. The most widely cited natural example of crystal–plastic deformation mechanisms localizing on brittle fractures is that of Segall and Simpson (1986). In their examples, the brittle and ductile events were separated by an unknown amount of time, and may not have formed during a progressive deformation event. The ductile deformation described by Segall and Simpson (1986) was strongly localized in the fractures, but gradients in ductile strain occurred in wall rocks adjacent to some of the fractures. These authors suggested that fluid access along wall-rock cracks caused reaction softening or hydrolytic weakening adjacent to the fractures, enhancing wall-rock ductility leading to the localized ductile strain gradients. This interpretation was later supported by Kronenberg et al. (1990b) on the basis of infrared spectroscopy and transmission electron microscopy analyses of the same rocks.

Relevant examples of ductile shear zones nucleating on precursor faults in laboratory experiments were reported by Tullis et al. (1990). They examined ductile shear-zone formation in quartzite, aplite and albite rocks that were prefaulted at low temperatures and high strain rates, and then briefly annealed at high temperatures. The annealed samples were then deformed at temperatures of 900–1100 °C, at an axial strain rate of $10^{-6}\ s^{-1}$. Although the fault gouge in these samples sintered and recrystallized during annealing, the ductile strain was strongly localized along the former faults in the aplite and albite rock, but not in the quartzite. Tullis et al. (1990) provided a two-fold explanation of this observation. First, the feldspar and quartz show different recovery mechanisms at these conditions. Feldspar undergoes recrystallization-accommodated dislocation creep, which in the fine-grained, sintered fault gouge allowed constant generation of small, strain-free new grains that were easily deformed. Thus, strain localized in these new grains. In contrast, for deformation under the same

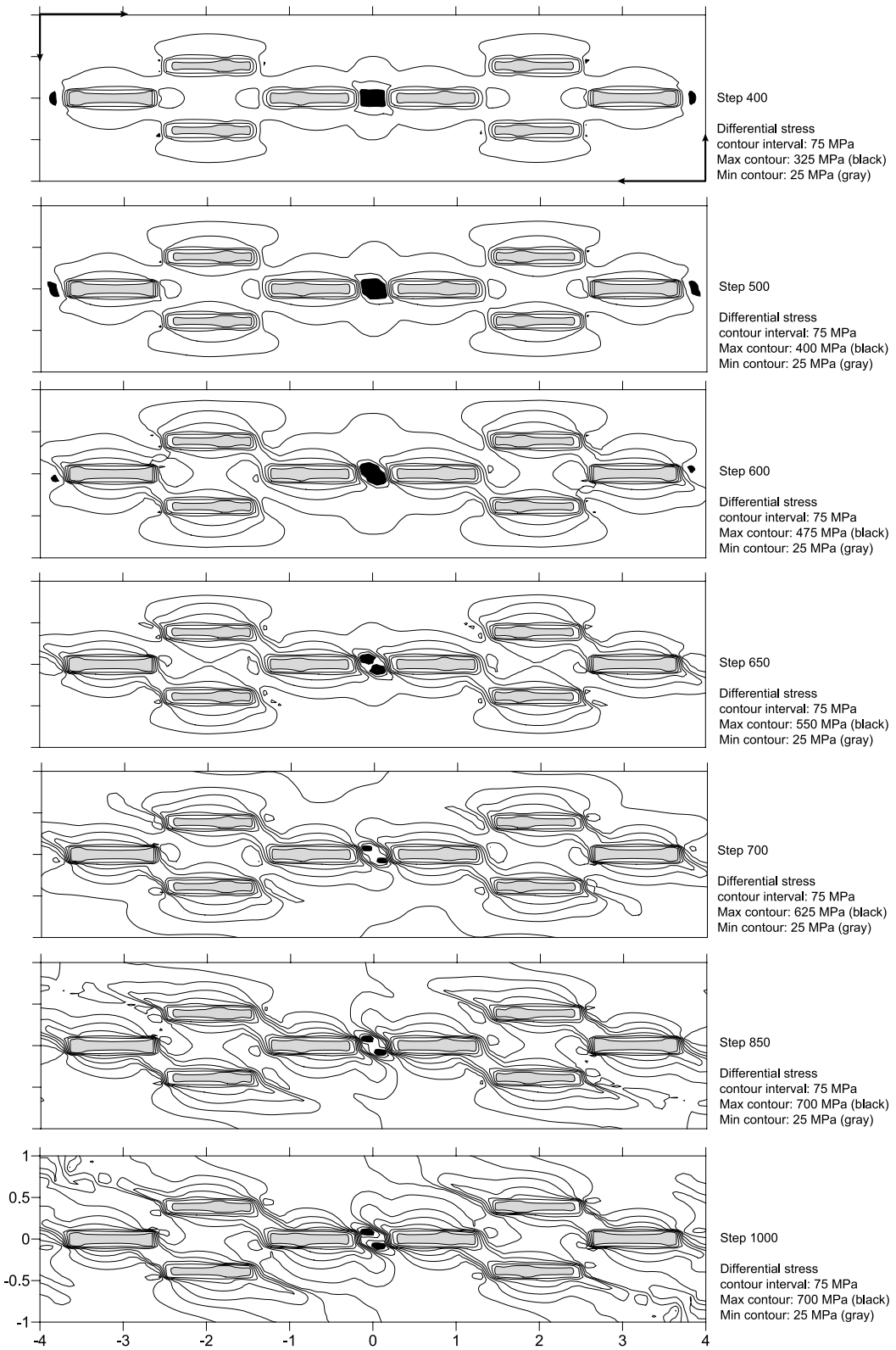

Fig. 9. Contours of differential stress ($\sigma_1 - \sigma_3$) in central sections through the numerical experiment at seven stages between steps 400 and 1000. Contour of maximum differential stress filled black, contour of minimum differential stress (biotite grains) filled gray. Note the high values of differential stress between the biotite grains.

conditions quartz undergoes climb-accommodated dislocation creep, which generates new recrystallized grains by progressive subgrain rotation. These new grains have similar dislocation densities to those of the subgrains from which they are derived, and their strength is similar to the original grains. Thus, strain did not localize in the new quartz grains. The second part of the explanation concerns the ease with which feldspar fractures relative to quartz, owing to its two good cleavages. Tullis and Yund (1987) showed that feldspars undergo more extreme grain size reduction than quartz during cataclasis. The tendency for faults in the aplite to follow feldspar as opposed to quartz grains led to greater grain-size reduction in the feldspar in the experiments of Tullis et al. (1990), and strain localized in the fine-grained feldspar during subsequent high temperature deformation. Tullis et al. (1990) noted that the tendency for feldspar to localize ductile strain along preexisting faults or fractures should be limited to rocks in which feldspar forms a stress-supporting framework, as in the northern marginal unit of the San José pluton.

The studies by Segall and Simpson (1986) and Tullis et al. (1990), in addition to the present study, illustrate the importance of brittle structures as sites of initiation of ductile shear zones. In the case of the San José pluton, a mylonitic foliation developed from initial fracturing, which raises the question of how many pervasively foliated mylonites in feldspar-rich rocks may have formed this way.

6.2. Preservation of microstructural relations

Recognition of a 'brittle–ductile transition' in the marginal northern unit would not have been possible without preservation of key microstructures. Although we suggest that the marginal northern unit was deformed at temperatures near the wet tonalite solidus ($T \sim 680$ °C at 300 MPa; Wyllie, 1977; Schmidt and Thompson, 1996), the subtle microstructures formed in these rocks are remarkably well preserved. The probability of preserving subtle microstructures is considerably enhanced if differential stress, strain rate and temperature are rapidly reduced more or less simultaneously across the deformation zone (e.g. Knipe, 1989; Prior et al., 1990; White and Mawer, 1992; Handy et al., 2001). Johnson et al. (2003) concluded that the brittle/crystal–plastic deformation in the marginal northern unit was caused largely or entirely by emplacement of the central unit of the tonalite into the partially crystallized northern unit. Thus, emplacement-related differential stress and strain rate would have dropped rapidly and simultaneously, immediately after emplacement had concluded. In addition, the pluton intruded rocks at temperatures consistent with greenschist-facies grade of regional metamorphism (Johnson et al., 2003), and the marginal northern unit was probably much hotter at the time deformation ceased. The resulting temperature gradient between the pluton and wall rocks would have caused a relatively rapid temperature drop in the marginal northern unit, in concert with the drop in differential stress and strain rate. Furthermore, the distance between the central unit and the marginal northern unit (>2 km) probably precluded sufficient reheating of the latter, minimizing destruction of the preserved microstructures through recovery processes. Thus, the multi-pulse nature of the pluton, the relatively low temperature of the surrounding wall rocks, and the pluton's late emplacement timing relative to regional ductile strain accumulation have all contributed to the unusual preservation of microstructures defining the deformation gradient in the marginal northern unit.

6.3. Evidence for high strain rates

The evidence for brittle deformation in the marginal northern unit of the San José pluton at relatively high temperatures, within an emplacement-related kinematic setting, raises the possibility of deformation at relatively high strain rates. Strain rates in rocks can be directly estimated if velocity boundary conditions (or the finite strain state) and the duration of deformation are known. Alternatively, if the temperature during deformation is known, the deformation microstructures can be compared with those from laboratory deformation experiments in an attempt to infer flow stresses and strain rates. We do not know the velocity boundary conditions of deformation (or the finite strain state) in the marginal northern unit, nor the precise time interval over which deformation occurred, and so we cannot make a direct estimate of strain rates. Although we have a rough estimate of the temperature (~680 °C) during at least part of the deformation, we are not certain how to extrapolate experimentally determined flow laws to these polymineralic rocks, nor the relevance of these flow laws to melt-present, cataclastic flow. Several recent studies have used microstructural observations in quartzites as a basis for applying laboratory-derived quartzite flow laws to naturally deformed rocks (e.g. Stöckhert et al., 1999; Hirth et al., 2001). However, few studies have attempted this application to polymineralic rocks (e.g. Yoshinobu and Hirth, 2002).

We use the following information to bracket likely strain rates during deformation of the marginal northern unit: (1) a brief comparison of feldspar microstructures in naturally and experimentally deformed rocks to those in the marginal northern unit; (2) previous studies of strain rates associated with pluton emplacement; and (3) theoretical studies of emplacement-related strain rates. Although we can only confidently bracket the bulk strain rate to within three orders of magnitude, we use this range to discuss the effects of strain rate partitioning on the microstructural evolution of these rocks.

6.3.1. Comparison of feldspar microstructures

Assuming that the temperature in the marginal northern unit at the time of deformation initiation was near the solidus temperature of wet tonalite (~680 °C at 300 MPa),

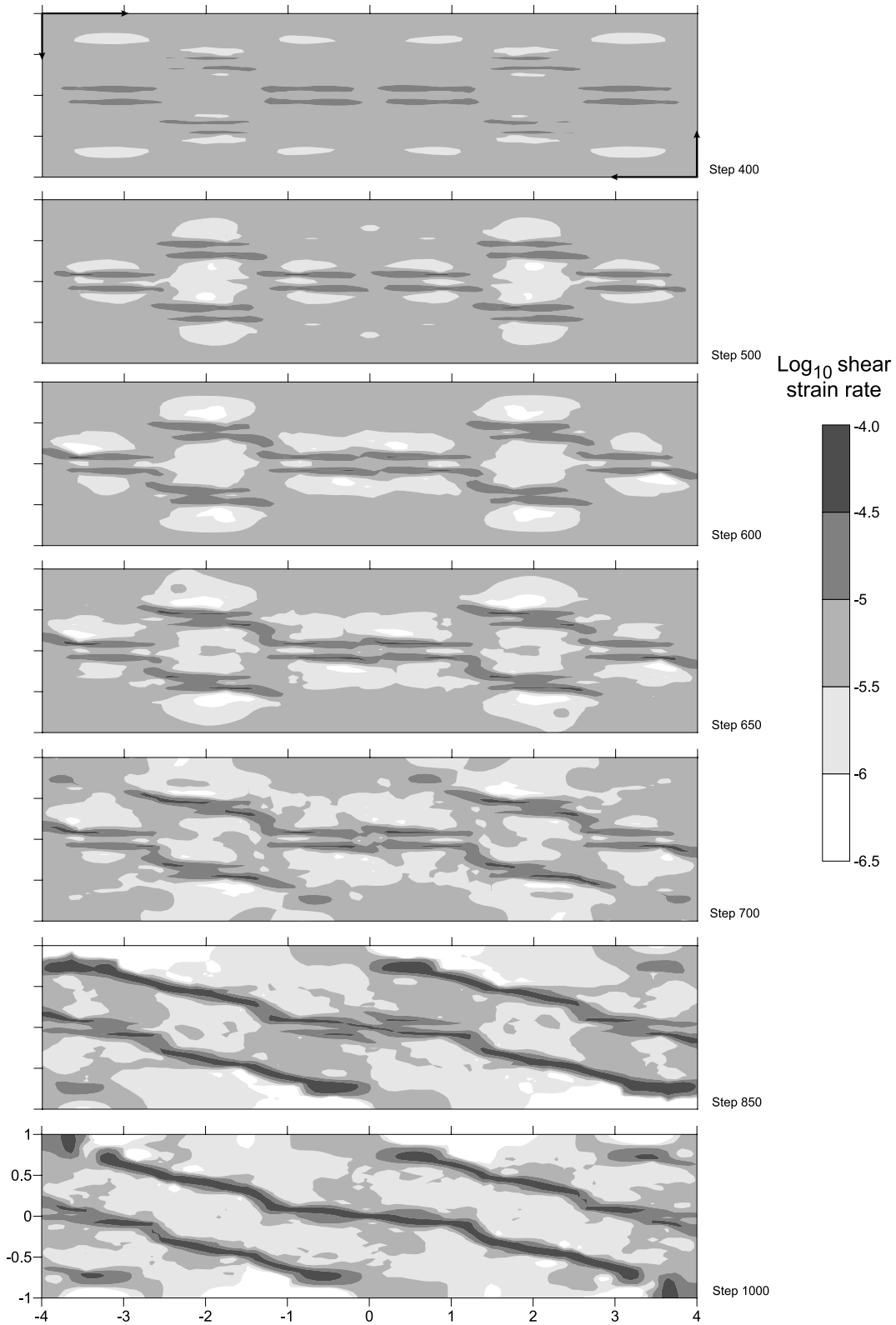

Fig. 10. Shaded contours of shear strain rate ($1/2[(\partial V_x/\partial z) + (\partial V_z/\partial x)]$) in central sections through the numerical experiment at seven stages between steps 400 and 1000. Note partitioning of higher strain rates into the biotite and linked zones of plastic failure, and associated drop in background strain rate throughout the surrounding matrix.

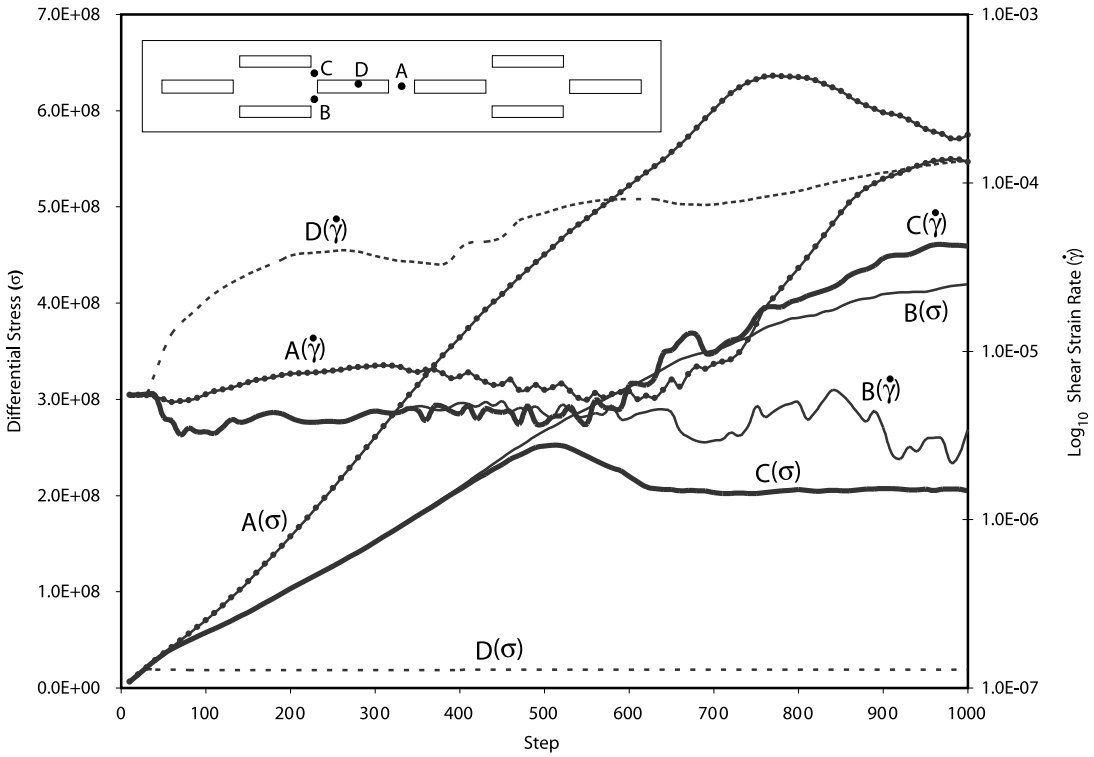

Fig. 11. Plot of progressive evolution of differential stress and shear strain rate at locations A–E in the model (inset). For each of these points, the curve for differential stress in denoted by (σ), and the curve for shear strain rate is denoted by ($\dot{\gamma}$).

and bulk strain rates were in the normally accepted tectonic range of 10^{-13}–10^{-15} s^{-1}, dislocation creep would likely have been the dominant deformation mechanism in plagioclase (e.g. Tullis, 1983; Simpson, 1985; Fitz Gerald and Stünitz, 1993; Pryer, 1993; Tullis, 2002). At these temperatures, naturally deformed plagioclase generally shows widespread grain boundary migration and in some instances subgrain formation, suggesting that recrystallization-accommodated and possibly climb-accommodated dislocation creep have occurred (Tullis and Yund, 1985). Although fracturing of feldspar has been documented in rocks deformed at upper amphibolite facies conditions (Fitz Gerald and Stünitz, 1993), the degree of fracturing is not as pronounced as that recorded in the marginal northern unit of the San José pluton. Plagioclase microstructures grossly similar to those in the marginal northern unit were developed in Enfield aplite experimentally deformed at temperatures of 800 °C, and strain rates of $\sim 10^{-6}$ s^{-1} (Dell'Angelo and Tullis, 1996). These experiments showed transitional behavior of feldspar between semi-brittle flow and recrystallization-accommodated dislocation creep. The above observations suggest that the marginal northern unit was deformed at rates faster than those normally associated with regional deformation ($\sim 10^{-13}$ s^{-1}), but probably at rates slower than those of the above-mentioned experimental study ($\sim 10^{-6}$ s^{-1}).

6.3.2. Pluton emplacement and strain rates

A growing body of evidence suggests that strain rates associated with pluton construction are fast relative to regional tectonic strain rates, regardless of the mechanism of magma ascent and emplacement (e.g. Clemens and Mawer, 1992; Paterson and Tobisch, 1992; Karlstrom et al., 1993; Weinberg and Podladchikov, 1995; Pavlis, 1996; Petford, 1996; Fernandez and Castro, 1999; McCaffrey et al., 1999; Handy et al., 2001; Johnson et al., 2001; Gerbi et al., 2004). For example, rates on the order of 10^{-11}–10^{-12} s^{-1} have been suggested for deformation in the aureoles of the East Piute and Old Woman plutons in southern California (Karlstrom et al., 1993; McCaffrey et al., 1999). John and Blundy (1993) estimated strain rates of 10^{-13} s^{-1} for ductile deformation in the aureole of the Adamello massif, Italy. Nyman et al. (1995) suggested that strain rates may have been of the order of 10^{-12} s^{-1} in the aureole of the Papoose Flat pluton, eastern California. Fernandez and Castro (1999) suggested that strain rates of 10^{-10}–10^{-11} s^{-1} formed in local 'kink-like' openings during magma emplacement. These strain rates are similar to the rates of 10^{-10}–10^{-13} s^{-1} suggested by Schmid (1989) and 10^{-9}–10^{-11} s^{-1} suggested by White and Mawer (1992), for some mylonite zones.

Johnson et al. (2001) and Gerbi et al. (2004) used analytical expressions for axial strain rates in the aureoles of expanding spheroids to estimate wall-rock strain rates

associated with the early stages of dike-fed pluton growth. Their modeling suggests that strain rates can reach sustained values of $\sim 10^{-7.5}$ s^{-1} or higher.

6.3.3. Summary

Considering the available evidence we suggest that the central unit was emplaced as a single pulse, and on the basis of the information presented above we estimate that emplacement-related deformation of the marginal northern unit occurred at strain rates between 10^{-8} and 10^{-11} s^{-1}, although rates during the early stages of deformation may have been much higher (Johnson et al., 2001; Gerbi et al., 2004). This spread of three orders of magnitude is not satisfying as a bulk-rate estimate. However, the modeling of Johnson et al. (2001) and Gerbi et al. (2004) shows that strain rates decrease with time at the margin of an 'expanding' pluton, and so the bulk rate may well have spanned several orders of magnitude, conceivably starting at 10^{-8} s^{-1} and decreasing to 10^{-11} s^{-1}. Strain rates may also vary spatially by up to three orders of magnitude, as shown in our numerical modeling (Figs. 10 and 11) and previous theoretical (e.g. Tullis et al., 1991; Handy et al., 1999) and experimental work (e.g. Jordan, 1987; Ross et al., 1987; Olgaard, 1990; Tullis et al., 1990; Bons and Cox, 1994; Rosenberg and Handy, 2000; Holyoke and Tullis, 2001). Therefore, trying to further constrain the bulk strain rate experienced by these rocks may provide less insight than exploring how rates might have partitioned between, say, 10^{-8} and 10^{-11} s^{-1} during progressive deformation.

An important implication from this discussion is that microstructures observed in single thin sections may reflect strain rates that span up to three orders of magnitude or more, depending on the degree of strain rate partitioning during deformation. Perhaps of more importance, strain rate partitioning of this magnitude or higher should be expected on a range of scales, which could lead to an overestimate or underestimate of bulk strain rates depending on where microstructural data are collected in a deformed sequence of rocks. On the basis of our microstructural observations and numerical experiments, as well as laboratory experiments on biotite-bearing rocks (e.g. Shea and Kronenberg, 1992, 1993; Holyoke and Tullis, 2001; Tullis, 2002), we suggest that biotite-rich layers in a deforming sequence of rocks may commonly deform at strain rates markedly higher than the bulk rate.

7. Conclusions

Although phyllosilicates have long been recognized as the weakest minerals in shear in most crustal rocks, relatively few studies have investigated their mechanical significance for shear initiation and localization leading to fabric development. Microstructural observations suggest that biotite was the weakest mineral in the deforming carapace of a tonalite pluton, and that it initiated and localized microfractures in a stress-supporting plagioclase framework. These microfractures evolved into ductile microshear zones, along which biotite grains coalesced to ultimately form a mylonitic foliation at the highest strains. Thus, the rocks preserve evidence for a progressive transition from brittle to ductile flow, the transition being controlled largely by mechanical and possibly chemical redistribution of biotite in concert with other weakening mechanisms (e.g. grain-size reduction of feldspar). Numerical experiments designed to investigate the role of biotite in initiating and localizing deformation illustrate the stress and strain-rate evolution that might be expected in initially homogeneous rocks containing biotite grains. The results of these experiments show the important role played by weak minerals in developing compositional layering that serves to reduce the material's bulk strength. These numerical experiments also provide insight into the degree to which strain rates may partition among different minerals in polymineralic rocks. Thus, microstructures in a single zone of deformation (or a single thin section) may reflect strain rates spanning three orders of magnitude or more, and strain rates determined by relating microstructures in deformed rocks to mineral flow laws derived from laboratory experiments may not reflect the bulk strain rate during deformation.

Acknowledgements

We acknowledge support of NSF Grant EAR-0087661, and thank Scott Paterson and Chris Gerbi for helpful comments prior to submission. We thank Aaron Yoshinobu and Aaron Stallard for helpful reviews of the submitted manuscript, and Jan Tullis for commenting on the final version.

References

Ashby, M.F., Hallam, S.D., 1986. The failure of brittle solids containing small cracks under compressive stress states. Acta Metallurgica 34, 497–510.

Bauer, P., Palm, S., Handy, M.R., 2000. Strain localization and fluid pathways in mylonite: inferences from in situ deformation of a water-bearing quartz analogue (norcamphor). Tectonophysics 320, 141–165.

Bell, T.H., 1981. Foliation development—the contribution, geometry and significance of progressive, bulk, inhomogeneous shortening. Tectonophysics 75, 273–296.

Bons, P.D., Cox, S.J.D., 1994. Analogue experiments and numerical modeling on the relation between microgeometry and flow properties of polyphase materials. Materials Science and Engineering A175, 237–245.

Bons, P.D., Urai, J.L., 1994. Experimental deformation of two-phase rock analogues. Materials Science and Engineering A175, 221–229.

Bons, P.D., Jessell, M.W., 1999. Micro-shear zones in experimentally deformed octachloropropane. Journal of Structural Geology 21, 323–334.

Brown, M., Solar, G.S., 1998. Shear-zone systems and melts: feedback

relations and self-organization in orogenic belts. Journal of Structural Geology 20, 211–227.

Burg, J.-P., 1999. Ductile structures and instabilities: their implication for Variscan tectonics in the Ardennes. Tectonophysics 309, 1–25.

Burg, J.-P., Vigneresse, J.L., 2002. Non-linear feedback loops in the rheology of cooling-crystallizing felsic magma and heating-melting felsic rock. In: De Meer, S., Drury, M.R., De Bresser, J.H.P., Pennock, G.M. (Eds.), Deformation Mechanisms, Rheology and Tectonics: Current Status and Future Perspectives. Geological Society, London, Special Publications 200, pp. 275–292.

Christiansen, P.P., Pollard, D.D., 1997. Nucleation, growth and structural development of mylonitic shear zones in granitic rock. Journal of Structural Geology 19, 1159–1172.

Clemens, J.D., Mawer, C.K., 1992. Granitic magma transport by fracture propagation. Tectonophysics 204, 339–360.

Coward, M.P., 1976. Strain within ductile shear zones. Tectonophysics 34, 181–197.

Dell'Angelo, L.N., Tullis, J., 1996. Textural and mechanical evolution with progressive strain in experimentally deformed aplite. Tectonophysics 256, 57–82.

Dey, T.N., Wang, C.-Y., 1981. Some mechanisms of microcrack growth and interaction in compressive rock failure. International Journal of Rock Mechanics and Mining Science and Geomechanical Abstracts 18, 199–209.

Ellis, S., Wissing, S., Pfiffner, A., 2001. Strain localization as a key to reconciling experimentally derived flow-law data with dynamic models of continental collision. International Journal of Earth Sciences 90, 168–180.

Fernandez, C., Castro, A., 1999. Pluton accommodation at high strain rates in the upper continental crust. The example of the central Exremadura batholith, Spain. Journal of Structural Geology 21, 1143–1150.

Fitz Gerald, J.D., Stünitz, H., 1993. Deformation of granitoids at low metamorphic grade. I: reactions and grain size reduction. Tectonophysics 221, 269–297.

Gapais, D., Bale, P., Choukroune, P., Cobbold, P.R., Mahjoub, Y., Didier, M., 1987. Bulk kinematics from shear zone patterns: some field examples. Journal of Structural Geology 9, 635–646.

Gastil, R.G., Phillips, R.P., Allison, E.C., 1975. Reconnaissance geology of the State of Baja California. Geological Society of America Memoir 140, 170pp.

Gerbi, C.C., Johnson, S.E., Paterson, S.R., 2004. Implications of rapid, dike-fed pluton growth for host-rock strain rates and emplacement mechanisms. Journal of Structural Geology 26, 583–594.

Goodwin, L.B., Tikoff, B., 2002. Competency contrast, kinematics, and the development of foliations and lineations in the crust. Journal of Structural Geology 24, 1065–1086.

Goodwin, L.B., Wenk, H.-R., 1995. Development of phyllonite from granodiorite: mechanisms of grain-size reduction in the Santa Rosa mylonite zone, California. Journal of Structural Geology 17, 689–707.

Gottschalk, R.R., Kronenberg, A.K., Russell, J.E., Handin, J., 1990. Mechanical anisotropy of gneiss: failure criterion and textural sources of directional behavior. Journal of Geophysical Research 95, 21613–21634.

Hacker, B.R., Christie, J.M., 1990. Brittle/ductile and plastic/cataclastic transitions in experimentally deformed and metamorphosed amphibolite. In: Duba, A., Durham, W., Handin, W., Wang, H. (Eds.), The Brittle–Ductile Transition. American Geophysical Union Geophysical Monograph 56, pp. 127–147.

Handy, M.R., 1990. The solid-state flow of polymineralic rocks. Journal of Geophysical Research 95, 8647–8661.

Handy, M.R., 1994. The energetics of steady state heterogeneous shear in mylonitic rock. Materials Science and Engineering A175, 261–272.

Handy, M.R., Wissing, S.B., Streit, L.E., 1999. Frictional–viscous flow in mylonite with varied bimineralic composition and its effect on lithospheric strength. Tectonophysics 303, 175–191.

Handy, M.R., Mulch, A., Rosenau, M., Rosenberg, C.L., 2001. The role of fault zones and melts as agents of weakening, hardening and differentiation of the continental crust: a synthesis. In: Holdsworth, R.E. Strachan, R.A. Magloughlin, J.F. Knipe R.J. (Eds.), The Nature and Tectonic Significance of Fault Zone Weakening. Geological Society, London, Special Publication 186, 305–332.

Hirth, G., Teyssier, C., Dunlap, J., 2001. An evaluation of quartzite flow laws based on comparisons between experimentally and naturally deformed rocks. International Journal of Earth Sciences 90, 77–87.

Hobbs, B.E., Mühlhaus, H.-B., Ord, A., 1990. Instability, softening and localization of deformation. In: Knipe, R.J., Rutter, E.H. (Eds.), Deformation Mechanisms, Rheology and Tectonics. Geological Society Special Publication 54, pp. 143–165.

Holyoke, C.W. III, Tullis, J., 2001. Initiation of ductile shear zones. Geological Society of America Abstracts with Programs 33(6), A-324.

Holyoke, C.W. III, Rushmer, T., 2002. An experimental study of grain scale melt segregation mechanisms in two common crustal rock types. Journal of Metamorphic Geology 20, 493–512.

Horii, H., Nemat-Nasser, S., 1986. Brittle failure in compression: splitting, faulting and brittle–ductile transition. Philosophical Transactions of the Royal Society of London, A 319, 337–374.

Itasca Consulting Group, Inc., 2002. FLAC^{3D}: Fast Lagrangian Analysis of Continua, Version 2.10, Itasca Consulting Group, Inc., Minneapolis.

Jiang, D., White, J.C., 1995. Kinematics of rock flow and the interpretation of geological structures, with particular reference to shear zones. Journal of Structural Geology 17, 1249–1265.

John, B.E., Blundy, J.D., 1993. Emplacement-related deformation of granitoid magmas, southern Adamello massif, Italy Geological Society of America Bulletin 105, 1517–1541.

Johnson, S.E., Tate, M.C., Fanning, C.M., 1999. New geological and SHRIMP U–Pb zircon data in the Peninsular Ranges batholith, Baja California, México: evidence for a suture? Geology 27, 743–746.

Johnson, S.E., Albertz, M., Paterson, S.R., 2001. Growth rates of dike-fed plutons: are they compatible with observations in the middle and upper crust? Geology 29, 727–730.

Johnson, S.E., Fletcher, J.M., Fanning, C.M., Vernon, R.H., Paterson, S.R., Tate, M.C., 2003. Structure, emplacement and in-situ expansion of the San José tonalite pluton, Peninsular Ranges batholith, Baja California, México. Journal of Structural Geology 25, 1933–1957.

Jordan, P., 1987. The deformational behaviour of bimineralic limestone—halite aggregates. Tectonophysics 135, 185–197.

Jordan, P., 1988. The rheology of polymineralic rocks—an approach. Geologische Rundschau 77, 285–294.

Karlstrom, K.E., Miller, C.F., Kingsbury, J.A., Wooden, J.L., 1993. Pluton emplacement along an active ductile thrust zone, Piute Mountains, southeastern California: interaction between deformational and solidification processes. Geological Society of America Bulletin 105, 213–230.

Kirby, S.H., 1985. Rock mechanics observations pertinent to the rheology of the continental lithosphere and the localization of strain along shear zones. Tectonophysics 119, 1–27.

Knipe, R.J., 1989. Deformation mechanisms—recognition from natural tectonites. Journal of Structural Geology 11, 127–146.

Kranz, R.L., 1983. Microcracks in rocks: a review. Tectonophysics 100, 449–480.

Kronenberg, A.K., Kirby, S.H., Pinkston, J., 1990a. Basal slip and mechanical anisotropy of biotite. Journal of Geophysical Research 95, 19257–19278.

Kronenberg, A.K., Segall, P., Wolf, G.H., 1990. Hydrolytic weakening and penetrative deformation within a natural shear zone. In: Duba, A., Durham, W., Handin, W., Wang, H. (Eds.), The Brittle–Ductile Transition. American Geophysical Union Geophysical Monograph 56, pp. 21–36.

Lama, R.D., Vutukuri, V.S., 1978. Handbook on Mechanical Properties of Rocks, Volume II. Series on Rock and Soil Mechanics, Vol. 3, No. 1, Trans Tech Publications, Switzerland, 481pp.

Lin, P., Logan, J.M., 1991. The interaction of two closely spaced cracks: a rock model study. Journal of Geophysical Research 96, 21667–21675.

Mancktelow, N.S., 1985. The Simplon Line: a major displacement zone in the western Lepontine Alps. Eclogae Geologicae Helvetiae 78, 73–96.

McCaffrey, K.J.W., Miller, C.F., Karlstrom, K.E., Simpson, C., 1999. Synmagmatic deformation patterns in the Old Women Mountains, SE California. Journal of Structural Geology 21, 335–349.

McLaren, A.C., Pryer, L.L., 2001. Microstructural investigation of the interaction and interdependence of cataclastic and plastic mechanisms in feldspar crystals deformed in the semi-brittle field. Tectonophysics 335, 1–15.

Murray, J.D., 1978. The structure and petrology of the San José pluton, northern Baja California, México. Unpublished Ph.D. thesis. Pasadena, California Institute of Technology, 709pp.

Nemat-Nasser, S., Horii, H., 1982. Compression-induced non-planar crack extension with application to splitting, exfoliation and rockburst. Journal of Geophysical Research 87, 6805–6821.

Nicholson, R., Pollard, D.D., 1985. Dilation and linkage of echelon cracks. Journal of Structural Geology 7, 583–590.

Nyman, M.W., Law, R.D., Morgan, S.S., 1995. Conditions of contact metamorphism, Papoose Flat Pluton, eastern California, USA: implications for cooling and strain histories. Journal of Metamorphic Geology 13, 627–643.

Olgaard, D.L., 1990. The role of second phase in localizing deformation. In: Knipe, R.J., Rutter, E.H. (Eds.), Deformation Mechanisms, Rheology and Tectonics. Geological Society Special Publication 54, pp. 175–181.

Park, Y., Means, D., 1996. Direct observation of deformation processes in crystal mushes. Journal of Structural Geology 18, 847–858.

Passchier, C.W., 1986. Flow in natural shear zones—the consequences of spinning flow regimes. Earth and Planetary Science Letters 77, 70–80.

Passchier, C.W., Druguet, E., 2002. Numerical modelling of asymmetric boudinage. Journal of Structural Geology 24, 1789–1803.

Paterson, S.R., Tobisch, O.T., 1992. Rates of processes in magmatic arcs: implications for the timing and nature of pluton emplacement and wall rock deformation. Journal of Structural Geology 14, 291–300.

Pavlis, T.L., 1996. Fabric development in syn-tectonic intrusive sheets as a consequence of melt-dominated flow and thermal softening of the crust. Tectonophysics 253, 1–31.

Petford, N., 1996. Dykes or diapirs? Royal Society of Edinburgh Transactions: Earth Sciences 87, 105–114.

Poirier, J.P., 1980. Shear localization and shear instability in materials in the ductile field. Journal of Structural Geology 2, 135–142.

Price, R.H., 1982. Effects of anhydrite and pressure on the mechanical behavior of synthetic rocksalt. Geophysical Research Letters 9, 1029–1032.

Prior, D.J., Knite, R.J., Handy, M.R., 1990. Estimates of the rates of microstructural changes in mylonites. In: Knipe, R.J., Rutter, E.H. (Eds.), Deformation Mechanisms, Rheology and Tectonics. Geological Society Special Publication 54, pp. 309–319.

Pryer, L.L., 1993. Microstructures in feldspars from a major crustal thrust zone: the Grenville Front, Ontario, Canada. Journal of Structural Geology 15, 21–36.

Ramsay, J.G., 1980. Shear zone geometry: a review. Journal of Structural Geology 2, 83–99.

Ramsay, J.G., Graham, R.H., 1970. Strain variation in shear belts. Canadian Journal of Earth Sciences 7, 786–813.

Rawling, G.C., Baud, P., Wong, T.-f., 2002. Dilatency, brittle strength, and anisotropy of foliated rocks: experimental deformation and micro-mechanical modeling. Journal of Geophysical Research 107(B10) DOI: 10.1029/2001JB000472.

Rosenberg, C.L., Handy, M.R., 2000. Syntectonic melt pathways during simple shearing of a partially molten rock analogue. Journal of Geophysical Research 105, 3135–3149.

Ross, J.V., Bauer, S.J., Hansen, F.D., 1987. Textural evolution of synthetic anhydrite–halite mylonites. Tectonophysics 140, 307–326.

Rutter, E.H., 1999. On the relationship between the formation of shear zones and the form of the flow law for rocks undergoing dynamic recrystallization. Tectonophysics 303, 147–158.

Schmid, S.M., 1989. Episodes in Alpine orogeny. Geological Society of America Abstracts with Programs 21, A28.

Schmidt, K.L., Paterson, S.R., 2002. A doubly vergent fan structure in the Peninsular Ranges batholith: transpression or local complex flow around a continental margin buttress? Tectonics 21, 2004.

Schmidt, M.W., Thompson, A.B., 1996. Epidote in calc-alkaline magmas: an experimental study of stability, phase relationships, and the role of epidote in magmatic evolution. American Mineralogist 81, 462–474.

Segall, P., Pollard, D.D., 1980. Mechanics of discontinuous faults. Journal of Geophysical Research 85, 4337–4350.

Segall, P., Pollard, D.D., 1983. Nucleation and growth of strike slip faults in granite. Journal of Geophysical Research 88, 555–568.

Segall, P., Simpson, C., 1986. Nucleation of ductile shear zones on dilatant fractures. Geology 14, 56–59.

Shea, W.T. Jr, Kronenberg, A.K., 1992. Rheology and deformation mechanisms of an isotropic mica schist. Journal of Geophysical Research 97, 15201–15237.

Shea, W.T. Jr, Kronenberg, A.K., 1993. Strength and anisotropy of foliated rocks with varied mica contents. Journal of Structural Geology 15, 1097–1121.

Sibson, R.H., 1986. Earthquakes and rock deformation in crustal fault zones. Annual Reviews in Earth and Planetary Sciences 14, 149–175.

Simpson, C., 1983. Strain and shape-fabric variations associated with ductile shear zones. Journal of Structural Geology 5, 61–72.

Simpson, C., 1985. Deformation of granitic rocks across the brittle–ductile transition. Journal of Structural Geology 7, 503–511.

Steif, P.S., 1984. Crack extension under compressive loading. Engineering Fracture Mechanics 20, 463–473.

Stöckhert, B., Brix, M.R., Kleinschrodt, R., Hurford, A.J., Wirth, R., 1999. Thermochronometry and microstructures of quartz—a comparison with experimental flow laws and predictions on the temperature of the brittle–plastic transition. Journal of Structural Geology 21, 351–369.

Streit, J.E., Cox, S.F., 2002. Evolution of fracture networks in shear zones: insights from see-through experiments on biphenyl aggregates. Journal of Structural Geology 24, 107–122.

Stünitz, H., 1998. Syndeformational recrystallization—dynamic or compositionally induced? Contributions to Mineralogy and Petrology 131, 219–236.

Tharp, T.M., 1983. Analogies between the high-temperature deformation of polyphase rocks and the mechanical behavior of porous powder metal. Tectonophysics 96, T1–T11.

Tullis, J., 1983. Deformation of feldspars. In: Ribbe, P.H. (Ed.), Feldspar Mineralogy. Mineralogical Society of America. Reviews in Mineralogy 2, pp. 297–323.

Tullis, J., 1990. Experimental studies of deformation mechanisms and microstructures in quartzo-feldspathic rocks. In: Barbour, D., Meredith, P. (Eds.), Deformation Processes in Minerals, Ceramics, and Rocks. Mineralogical Society Series 1, pp. 190–227.

Tullis, J., 2002. Deformation of granitic rocks: experimental studies and natural examples. In: Karato, S.-i., Wenk, H.-R. (Eds.), Plastic Deformation of Minerals and Rocks. Mineralogical Society of America. Reviews in Mineralogy and Geochemistry 51, pp. 51–96.

Tullis, J., Yund, R., 1977. Experimental deformation of dry Westerly granite. Journal of Geophysical Research 82, 5705–5718.

Tullis, J., Yund, R., 1980. Hydrolytic weakening of experimentally deformed Westerly granite and Hale albite rock. Journal of Structural Geology 2, 439–451.

Tullis, J., Yund, R.A., 1985. Dynamic recrystallization of feldspar: a mechanism for ductile shear zone formation. Geology 13, 238–241.

Tullis, J., Yund, R.A., 1987. Transition from cataclastic flow to dislocation creep of feldspar: mechanisms and microstructures. Geology 15, 606–609.

Tullis, J., Dell'Angelo, L., Yund, R.A., 1990. Ductile shear zones from brittle precursors in feldspathic rocks: the role of dynamic recrystallization. In: Duba, A., Durham, W., Handin, W., Wang, H. (Eds.), The Brittle–Ductile Transition. American Geophysical Union Geophysical Monograph 56, pp. 67–82.

Tullis, T.E., Horowitz, F.G., Tullis, J., 1991. Flow laws of polyphase aggregates from end-member flow laws. Journal of Geophysical Research 96, 8081–8096.

Van Roermund, H., Lister, G.S., Williams, P.F., 1979. Progressive development of quartz fabrics in a shear zone from Monte Mucrone, Sesia-Lanzo Zone, Italian Alps. Journal of Structural Geology 1, 43–52.

Vermeer, P.A., deBorst, R., 1984. Non-associated plasticity for soils, concrete and rock. Heron 29, 1–62.

Vernon, R.H., 1975. Deformation and recrystallization of a plagioclase grain. American Mineralogist 60, 884–888.

Vernon, R.H., Johnson, S.E., Melis, E.A., 2004. Emplacement-related microstructures in the margin of a deformed pluton: the San José tonalite, Baja California, México. Journal of Structural Geology, in press (doi: 10.1016/j.jsg.2004.02.007).

Vigneresse, J.L., Tikoff, B., 1999. Strain partitioning during partial melting and crystallizing felsic magmas. Tectonophysics 312, 117–132.

Weinberg, R.F., Podladchikov, Y.Y., 1995. The rise of solid-state diapers. Journal of Structural Geology 17, 1183–1195.

White, J.C., Mawer, C.K., 1992. Deep-crustal deformation textures along megathrusts from Newfoundland and Ontario: implications for microstructural preservation, strain rates, and strength of the lithosphere. Canadian Journal of Earth Sciences 29, 328–337.

White, S.H., Burrows, S.E., Carreras, J.,Shaw, N.D.,Humphreys, F.J.,1980. On mylonites in ductile shear zones. Journal of Structural Geology 2, 175–187.

Wyllie, P.J., 1977. Crustal Anatexis: an experimental review. Tectonophysics 43, 41–71.

Yoshinobu, A.S., Hirth, G., 2002. Microstructural and experimental constraints on the rheology of partially molten gabbro beneath oceanic spreading centers. Journal of Structural Geology 24, 1101–1107.